Signal Simulation and Signal Processing for Multiple Reference Optical Coherence Tomography

Kai Neuhaus[a]*, Hrebesh Subhash[a]†, Roshan Dsouza[a], Josh Hogan[c], Carol Wilson[c] and Martin Leahy[a,b]

[a]Tissue Optics and Microcirculation Imaging Group, School of Physics, National University of Ireland, Galway, Ireland;
[b]Royal College of Surgeons (RCSI), Dublin, Ireland;
[c]Compact Imaging, Inc., 897 Independence Ave., Suite 5B, Mountain View, CA 94043 USA.

ABSTRACT

The generation of a synthetic MR-OCT signal is presented and compared to a real acquired signal. Multiple reference optical coherence tomography (MR-OCT) is a novel time-domain interferometric system. The MR-OCT principle is adding a partial mirror to extend the axial scan range, which effectively extends the scan depth for imaging. The actuation of the scan mirror required for time-domain OCT, was demonstrated to operate with a low cost miniature voice coil, such as a speaker extracted from a smartphone or CD/DVD pick-up system. Building a compact and cost-effective optical imaging system will enable affordable medical diagnosis at low-resource setting applications. The partial mirror recirculates multiple reflections (orders) into the interferometric system and the increase of optical path delay does increase the beat frequency of the interference signal. The synthesis of such an interference signal using a numerical method is described in this manuscript.

Keywords: signal processing, interferometry, optical coherence tomography, simulation, optical imaging

1. INTRODUCTION

Optical coherence tomography (OCT) has become a well-established tool in many medical areas, such as ophthalmology, dermatology, gastrointestinal endoscopy and intravascular imaging. Modern high specification OCT systems are expensive and have large form-factors mostly limited for stationary clinical applications. Multiple reference optical coherence tomography (MR-OCT) is a new technology that enables compact and affordable OCT systems. MR-OCT is a robust and cost-effective optical imaging solution, which can be manufactured with micro optical components and has the potential to be integrated using solid state design. The availability of micro optical components and the technology for high-volume manufacturing, such as for miniature cameras of smartphones and CD/DVD pick-up systems, offer low-cost production processes.

The moderate axial scan speeds due to the electro-mechanical actuation of the scanning mirror (SM) allows the use of low-spec electronic components for signal acquisition and signal processing. This makes MR-OCT suitable for low-resource settings of medical diagnostics and biometric applications.

The difference between TD-OCT and MR-OCT is, that MR-OCT uses a partial mirror (PM) in front of the scanning mirror (SM) of the reference arm of the interferometric system. In currently demonstrated MR-OCT systems[1] the PM is designed to reflect 80 percent of the light back to the SM, while the remaining 20 percent pass through the PM, back into the interferometric system for imaging. The distance between the SM and the PM can be adjusted and was demonstrated with about 50 μm. Due to the spring-mass system of the actuator of the SM the movement will be a simple harmonic motion. The light is reflected back and forth multiple times between the PM and the SM generating a composite reference signal. Each further reflection (order) corresponds to an increased path length in the reference arm which only interferes with light from the sample arm matching the path length. Consequently, there is a systematic increase in the magnitude of the scan range associated with the corresponding order of reflections from the reference arm.

*k.neuhaus2@nuigalway.ie
†hrebesh.molloysubhash@nuigalway.ie

In Fig. 1(a) a schematic of the MR-OCT system is shown. A first order reflection will have a path length of the distance between SM and the beam splitter (BS) interface. For a second order reflection the path length increases by z. Any higher order reflection will have a path length increased by nz due to the additional distance the light has to travel between the PM and the SM. Figure 4 explains the geometrical propagation of rays between the PM and the SM for the first and second order, and the subsequent increase by multiples of the distance z. Due to the increased scanning range for any higher order

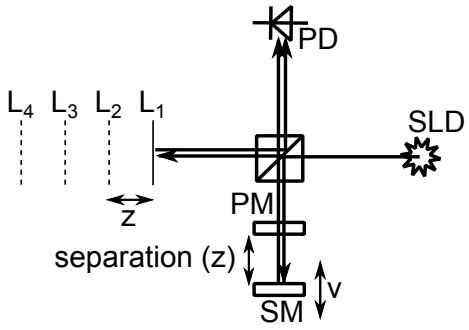

(a) Principle of MR-OCT showing the beam splitter (center), super-luminescent diode (SLD), photo detector (PD), partial mirror (PM), scanning mirror(SM), and different locations (L_n) of a sample mirror with separation (z).

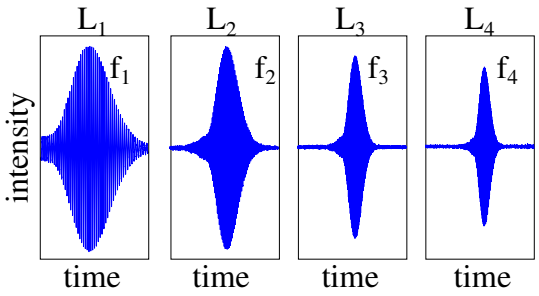

(b) Idealized signal traces showing four orders of interference signals occurring for four locations of the sample mirror (L_1,L_2,L_3,L_4). The interference signals have increasing frequencies f_1 to f_4. Note: In practice, because of the increasing virtual scan range, higher order traces show multiple order interference signals.

Figure 1: Overview of the operational principle of MR-OCT.

and the constant scan velocity v_R of the scanning mirror the frequency of the interference signal does increase with each order. The frequency for each order (Fig. 1(b)) follows the relation $f_n = f_1 \cdot n$, where f_1 is the frequency of the first order, n denotes the order number and f_n is the frequency of any higher order. These frequency properties are used to separate the orders by filtering the input signal with multiple band-pass filters (Fig. 2).

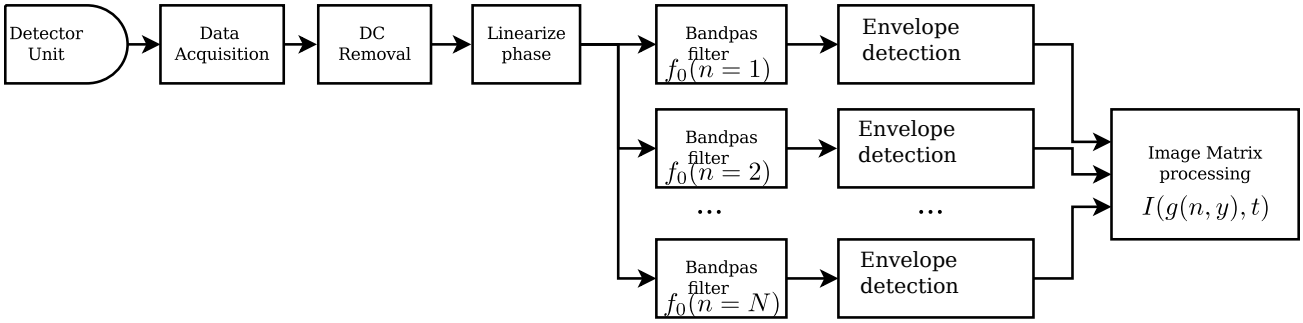

Figure 2: Signal processing flow for MR-OCT includes band pass filter with a center frequency f_0 for each order of reflection n with N for the amount of processed orders. The image matrix processing with the function g performs a correction of the wavenumber k for each A-line signal y and assembles a full B-frame I to display.

The different orders of reflections and the resulting composite signal contains the information of multiple depth layers of a sample. If the amplitude of the scanning mirror is Δz, the axial range of the related order of reflection n corresponds to Δzn. The 3^{rd} order reflection will therefore have an axial range of $3\Delta z$, which is three times larger than the actual scanning amplitude of the scanning mirror. After acquisition the signal for any higher order, and larger axial range, occur in the same time interval and are subsequently distorted in length (too short). The time interval corresponds to the wavenumber k and each signal can be corrected by $k(n) = nk$, which is performed in the image matrix processing (Fig. 3). The image matrix processing is also correcting the placement of a scan range related to the increased depth layer L (Fig. 1(a)), which is graphically indicated in Fig. 3.

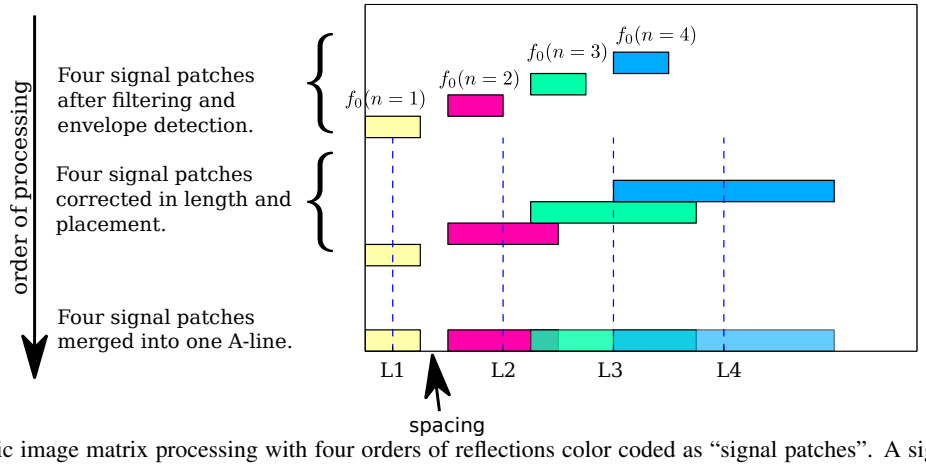

Figure 3: Schematic image matrix processing with four orders of reflections color coded as "signal patches". A signal patch is a data array of fixed sample length containing the OCT signal of the corresponding order of reflection. The graph indicates the processing steps to correct for length and placement of the signal patches and finally merging them into an A-line. The spacing between the scanning mirror and the partial mirror is typically larger than the maximum amplitude of the scanning mirror to avoid contact with the partial mirror during scanning. Subsequently the first order patch is shorter than the distance to the second order and a space between the signal patches occurs.

The amount of depth ranges to be processed can be controlled by signal processing. However, even with moderate scan speeds (currently reported to be approximately 400 Hz[1]) and expected sample rates (below 10 MHz), the filter process for separating the orders can consume a significant amount of time, due to the multitude filter units. Since multi-core processing units are available in tablet computers and smartphones, it may be possible to parallelize the processing of the filter process.

The maximum amount of depth layers detectable is limited by absorption and attenuation effects of the sample and the optical components. It is reported[1] that about 10 layers are possible, although under optimal conditions more layers may be achieved.

2. METHOD

The synthesis of an MR-OCT signal is based on the theory of TD-OCT signals, therefore a short review of selected parts of the equations are given here.

The theoretical expected average detector current $I(k,\omega)$ originating from two interfering wave fronts E_R and E_S is given[2] as:

$$I(k,\omega) = \frac{\rho}{2}\langle|E_R + E_S|^2\rangle. \tag{1}$$

The detector current depends on the wavenumber k and frequency of the light source ω, with ρ as detector responsivity.

After further deduction[2], ω is eliminated due to the heterodyne mixing effect. Otherwise the high-frequency of the light is not detectable directly by the detector. The complete solution[2] contains the DC term, the auto-correlation term and the cross-correlation term. In case of interference between reference arm and sample arm of an interferometer the cross-correlation term is the signal of interest.

Considering only the cross-correlation term[2] and ignoring the DC and auto-correlation term the detector current I can be written as:

$$I(k) = \frac{\rho}{2}\left[S(k)\sum_{n=1}^{N}\sqrt{R_R R_{S_n}}(\cos[2k(z_R - z_{S_n})])\right]. \tag{2}$$

The detector current is the sum over all reflecting elements R at a distance z from the beam splitter multiplied by the power spectral dependence of the light source $S(k)$,

The light source is assumed to have a Gaussian-shaped spectrum

$$S(k) = \frac{1}{\Delta k\,\sqrt{\pi}} \exp\left(-\left[\frac{(k-k_0)}{\Delta k}\right]^2\right) \tag{3}$$

with Δk corresponding to the bandwidth of the light source,

$$\Delta k = \frac{\pi}{\sqrt{\ln(2)}} \frac{\Delta\lambda}{\lambda^2}. \tag{4}$$

Equation (4) can be reshaped by using the full width half mean (FWHM) of a Gaussian to obtain the coherence length l_c:

$$l_c = \frac{2\sqrt{\ln 2}}{\Delta k} = \frac{2\ln(2)}{\pi} \frac{\lambda_0^2}{\Delta\lambda}. \tag{5}$$

The oscillatory term $\tilde{J}$ of the detector signal for a single reflecting layer is

$$\tilde{J} = \cos[2k(z_R - z_S)] = \cos[2k\Delta z]. \tag{6}$$

For only one reflecting layer the summing operation can be omitted which is useful to discuss only the sum of multiple reflections generated by the partial mirror.

The reference mirror is assumed to be moving with a velocity v_R and changing the distance z_R which results in the Doppler frequency[3]

$$f_D = 2v_R \frac{1}{\lambda}. \tag{7}$$

The movement of the reference mirror is often stated as linear, which simplifies the mathematical treatment. In this investigation the reference mirror was attached to a voice coil extracted from a CD/DVD pickup system, which will closely follow a harmonic motion due to the mass-spring system. The harmonic motion of the reference scanning mirror is $v_R = -A\omega_r \cos(\omega_r t + \phi_r)$, with A for the amplitude or the scan range, ω_r for the frequency and ϕ_r the phase.

With $k = \frac{2\pi}{\lambda}$ and the amplitude normalized, the oscillatory term can be written as:

$$\tilde{J}(t) = \cos[2\pi f_D\, t]. \tag{8}$$

Figure 4 shows the geometrical relation how each reflection due to the partial mirror does increase the path delay.

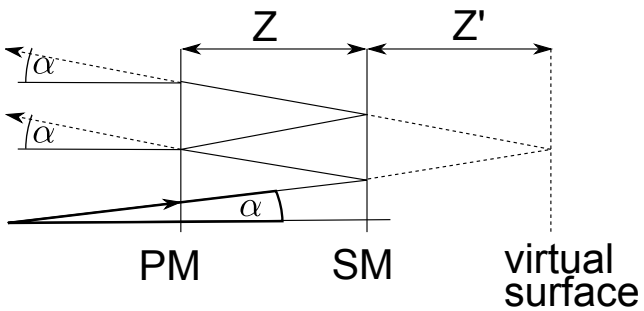

Figure 4: Geometrical representation of multiple reflections, visualizing a second reflection on PM. The drawing shows a reflection from PM re-drawn as a virtual surface. As z = z' the path delay for the second reflection is now 2z.

As shown in Fig. 4 the path delay z increases for the second reflection by Δz. Subsequently, the increase of the path delay for any higher order n is nz. Expanding Eq. (7) with $v = \frac{\Delta z}{\Delta t}$ and substitute Δz with $\Delta z n$:

$$f_D(n) = 2\frac{\Delta z}{\Delta t}\frac{n}{\lambda} = 2v_R\frac{n}{\lambda}; \quad n = 1,2,\ldots \tag{9}$$

which gives the Doppler frequency[4] for the path delay $\Delta z(n)$ and the length of the path delay for the nth reflection:

$$\Delta z(n) = \Delta z n; \quad n = 1,2,\ldots . \tag{10}$$

Rewriting the Eq. (6) incorporating n path delays:

$$\tilde{J}(\Delta t) = \sum_{n=1}^{N} \cos(2\pi f_D(n)\Delta t) \tag{11}$$

a sum of multiple frequency components for a single sample reflector can be computed. The different frequency of each component is used to separate the signals by filtering obtaining a series of signals.

The Gaussian component determines the peak position at k_0 of the envelope for each frequency component related to wavelength and bandwidth of the light source. For the purpose to synthesize an idealized signal any dispersion effects are neglected, and the Gaussian envelope related to a reflecting layer can be defined as:

$$S(z) = \exp\left(-\left[\frac{(z - z_0)}{l_c}\right]^2\right). \tag{12}$$

Using Eq. (12) a valid signal can be synthesized for the first order reflection (Fig. 5). For higher order reflections the centre position of the Gaussian envelope does shift according to Eq. (10). As the scan length increases (Eq. (10)), the FWHM of the Gaussian envelope will reduce by n:

$$S(z,n) = \exp\left(-\left[\frac{(z - (z_0 + \Delta z(n-1)))}{l_c/n}\right]^2\right). \tag{13}$$

The signal depends also on the scan mirror velocity v_R which will distort signal. The distortion is synthesized by using a look-up function K which displace the spatial data accordingly. Synthesizing a signal can now be performed by combining Eqs. (12) and (13) and creating the sum of all n reflections in Eq. (14):

$$I(t,z) = \cdot \sum_{n=1}^{N} K(v_R, S(z,n) \cdot \tilde{J}(t,n)). \tag{14}$$

For a SLED from Denselight Semiconductors (DL-CS3207a) a wavelength of $\lambda_0 = 1310$ nm and a bandwidth of $\Delta\lambda = 56$ nm it was possible to use the mathematical relation to estimate the actual scan range (amplitude of the harmonic motion) of the scan mirror.

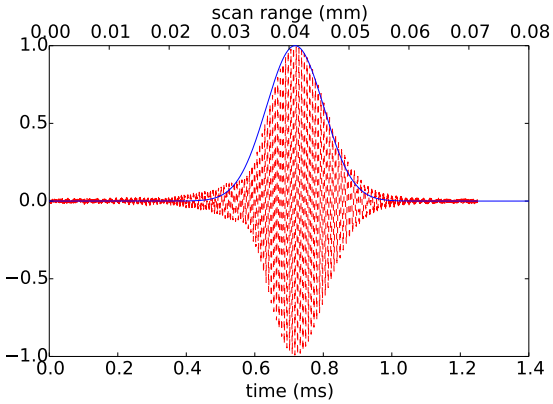

Figure 5: Calibrated Gaussian envelope (blue, solid) matching a real signal (red, dashed). It was possible to extract the scan width by fitting the Gaussian envelope based on the wavelength of the light source with about 70 µm.

3. RESULTS

The theoretical expected fundamental frequencies for each order n do not exactly match with the measured frequency (Fig. 6(b)) due to common expected dispersion effects, such as chromatic aberration and group delays in glass and air. The instability of the oscillation of the scan mirror will also distort the signal. For test purposes a CD/DVD pick-up coil was extracted from a decommissioned DVD-drive to excite the scan mirror with a frequency of 400 Hz. The voice coil was driven by a computer generated sinusoidal voltage via a pre-amplifier. The frequency stability of the voice coil appears to be sufficient for imaging[1].

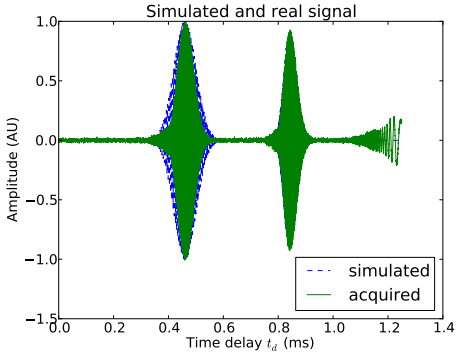

(a) Gaussian response for the 3^{rd} and 4^{th} order of a mirror placed in the sample arm of the MR-OCT.

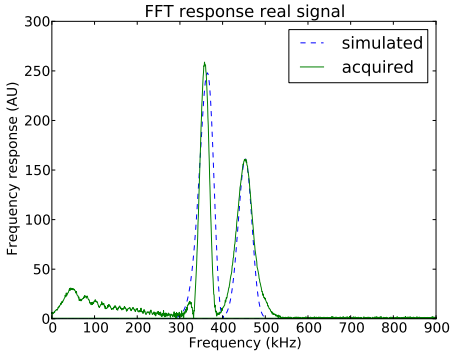

(b) Comparison of FFT between simulated and measured data.

Figure 6: The results show the measured and simulated data.

The strong reflection of a sample mirror generates a well-defined Gaussian response, as shown in Fig. 6(a). The signal synthesis did reproduce a similar characteristics compared to the acquired signal from the voice coil actuated system, confirming the validity of the current model. Such modeling of data can further be used to test filter characteristics and to improve the image processing and image quality.

4. CONCLUSION

A mathematical review of an MR-OCT signal was given and numerically reproduced for synthesizing such a signal. The results were compared to digitally acquired data set. The frequency spectrum of the simulated data followed closely the characteristics of the acquired signal from a voice-coil actuated system, confirming the currently proposed model. Such a model allows to generate other signals which can be used to investigate other signal characteristics and the performance of the signal processing. Further studies are planned to improve the model's accuracy and the relation to the mathematical properties. The usage of the model can reveal parallel patterns of the MR-OCT signal which can be used to improve the algorithmic implementation, which may lead to more efficient use of hardware such as tablet-computers and smartphones.

5. ACKNOWLEDGMENTS

This work was supported by Galway University Foundation, the University of Limerick Foundation, the National Biophotonics Imaging Platform (NBIP) Ireland funded under the Higher Education Authority PRTLI Cycle 4, co-funded by the Irish Government and the European Union – Investing in your future, and Compact Imaging, Inc. All authors have a financial interest in Compact Imaging, Inc.

REFERENCES

[1] Dsouza, R., Subhash, H., Neuhaus, K., Hogan, J., Wilson, C., and Leahy, M., "Dermascope assisted interactive patient interface for multiple reference optical coherence tomography," *Proc. SPIE* **8935**, 89350B–89350B–9 (2014).

[2] Drexler, W. and Fujimoto, J., [*Optical Coherence Tomography: Technology and Applications*], Biological and Medical Physics, Biomedical Engineering, Springer (2008).

[3] Brezinski, M., [*Optical Coherence Tomography: Principles and Applications*], Elsevier Science (2006).

[4] Dsouza, R., Subhash, H., Neuhaus, K., Hogan, J., Wilson, C., and Leahy, M., "Dermascope guided multiple reference optical coherence tomography," *Biomed Opt Express* **5**(9), 2870–2882 (2014).